Intrahepatic inflammatory IgA⁺PD-L1^{high} monocytes in hepatocellular carcinoma development and immunotherapy

Pil Soo Sung [1,2] Dong Jun Park,[2] Pu Reun Roh,[2] Kyoung Do Mun,[2] Sung Woo Cho,[2] Gil Won Lee,[2] Eun Sun Jung,[3] Sung Hak Lee,[4] Jeong Won Jang,[1] Si Hyun Bae,[5] Jong Young Choi,[1] Jonghwan Choi,[6] Jaegyoon Ahn,[7] Seung Kew Yoon[1,2]

ABSTRACT

Background IgA neutralizes pathogens to prevent infection at mucosal sites. However, emerging evidence shows that IgA contributes to aggravating inflammation or dismantling antitumor immunity in human diseased liver. The aim of this study was to elucidate the roles of inflammation-induced intrahepatic inflammatory IgA⁺ monocytes in the development of hepatocellular carcinoma (HCC).

Methods Patient cohorts including steatohepatitis cohort (n=61) and HCC cohort (n=271) were established. Patients' surgical and biopsy specimens were analyzed using immunohistochemistry. Multicolor flow cytometry was performed with a subset of patient samples. Single-cell RNA-Seq analysis was performed using Gene Expression Omnibus (GEO) datasets. Additionally, we performed in vitro differentiation of macrophages, stimulation with coated IgA, and RNA sequencing. Hepa1-6 cells and C57BL/6N mice were used to obtain HCC syngeneic mouse models.

Results Serum IgA levels were associated (p<0.001) with fibrosis progression and HCC development in patients with chronic liver diseases. Additionally, immunohistochemical staining of inflamed livers or HCC revealed IgA positivity in monocytes, with a correlation between IgA⁺ cell frequency and IgA serum levels. Compared with IgA⁻ monocytes, intrahepatic IgA⁺ monocytes expressed higher levels of programmed death-ligand 1 (PD-L1) in inflamed livers and in HCC tumor microenvironment. Single-cell RNA sequencing using NCBI GEO database indicated an upregulation in inflammation-associated genes in the monocytes of patients whose plasma cell *IGHA1* expression was greater than or equal to the median value. Bulk RNA sequencing demonstrated that in vitro stimulation of M2-polarized macrophages using coated IgA complex induced PD-L1 upregulation via YAP-mediated signaling. In vivo blockade of IgA signaling decreased the number of tumor-infiltrating IgA⁺PD-L1^{high} macrophages and increased the number of CD69⁺CD8⁺ T cells to enhance antitumor effects in HCC mice models.

Conclusions Overall, the findings of this study showed that serum IgA levels was correlated with intrahepatic and intratumoral infiltration of inflammatory IgA⁺PD-L1^{high} monocytes in chronic liver diseases and HCC, providing potential therapeutic targets.

Key messages

What is already known on this topic
⇒ Liver IgA⁺ plasma cells directly suppress cytotoxic T-lymphocyte (CTL) activation in vitro and in vivo, inducing CTL exhaustion and dismantlement of intrahepatic antitumor immunity.

What this study adds
⇒ We showed that serum IgA level is higher in hepatocellular carcinoma (HCC) patients and is associated with intrahepatic infiltration of inflammatory IgA⁺PD-L1^{high} monocytes. These cells may be targeted by IgA neutralization/anti-PD-L1 to enhance the efficacy of immune-based therapy in HCC.

How this study might affect research, practice or policy
⇒ HCC is characterized by an increase in the number of immune-regulatory cells in tumor microenvironment (TME), which limits the effectiveness of immune-based therapy. Our findings give critical insight into the development of immunosuppressive TME in HCC and potential strategies to overcome it.

BACKGROUND

Primary liver cancer has the sixth highest prevalence among malignant tumors and is responsible for the third-highest cancer-related mortality globally. Hepatocellular carcinoma (HCC) accounts for approximately 80% of primary liver cancer cases,[1] with an 80% incidence increase globally in recent decades.[2] The survival of patients with various malignancies can be prolonged by immune checkpoint inhibitors, with or without tyrosine kinase inhibitors. However, nivolumab monotherapy, the first approved anti-programmed death (PD)-1 monoclonal antibody, only has an objective response rate (ORR) of <20% in HCC.[3–5] The Checkmate-040 study of unresectable HCC revealed that programmed death-ligand 1 (PD-L1) expression in >1% of tumor cells was

associated with a 28% ORR for nivolumab compared with a 16% ORR with PD-L1 expression in <1% of tumor cells.[6]

Representative intrahepatic pathological conditions with non-resolving inflammation include non-alcoholic fatty liver disease (NAFLD) and alcoholic liver disease (ALD). Non-resolving liver damage is followed by deregulated wound healing and excessive extracellular matrix deposition, resulting in liver fibrosis.[7] Innate immunity seems to be a major factor affecting this disease progression, with liver-resident macrophages (Kupffer cells) and monocyte-derived macrophages (MoMFs) playing major roles.[7–10] Traditionally, macrophages are classified into two main groups: classically activated macrophages (M1) and alternatively activated macrophages (M2).[10] However, recent studies, including single-cell sequencing, have shown that intrahepatic macrophages are plastic, and cannot be defined as M1 or M2 phenotypes.[11] Macrophages or surrounding tumors differentiate into tumor-associated macrophages (TAMs) with the progression of HCC, and their infiltration is associated with poor prognosis in HCC.[10 12] Interestingly, recent single-cell analyses have identified co-existing M1 and M2 signatures in TAMs, indicating that TAM phenotype may not be defined using the classical M1/M2 model.[13] Some previous studies have shown that HCC tumor microenvironment (TME) is infiltrated by PD-L1-expressing activated monocytes with protumoral features,[14 15] although the underlying mechanisms are poorly understood.

Macrophage phenotypic plasticity is well described in liver injury and repair.[16] During NAFLD progression, Kupffer cells and recruited blood-derived monocytes differentiate into proinflammatory macrophages.[16] Specifically, a recent study using human NAFLD liver demonstrated that gut-derived lipopolysaccharides (LPS) are abundantly present in the liver and may increase liver damage by activating monocytes/macrophages through toll-like receptor (TLR)-4 pathway.[17] These results suggest that TLR-engaged macrophages represent critical inflammatory mediators in patients with NAFLD. During stimulation by TLR ligands, Kupffer cells secrete CCL2 and recruit proinflammatory and profibrogenic MoMFs to establish a profibrogenic niche in affected liver.[10 18] This CCL2–CCR2 signaling axis may also be a significant target for monocyte recruitment in HCC TME.[10] CCR2 antagonist treatment was reported to effectively suppress HCC tumor growth in different murine models.[19]

A recent study demonstrated that Trem-2 regulates the transition of macrophage population during liver injury and fibrogenesis.[16] This transition was associated with the down-modulation of the proinflammatory phenotype, which did not occur in the absence of Trem-2.[16] Another study using scRNA-seq identified a previously unknown macrophage type in the fibrotic niche of the human diseased liver.[20] During uncontrolled chronic inflammation of diseased livers, profibrogenic TREM2+CD9+ scar-associated macrophages differentiate from circulating monocytes and expand in the fibrotic liver.[20] Collectively, these reports suggest that intrahepatic macrophage phenotype shifts from an inflammatory phenotype to an anti-inflammatory or profibrogenic phenotype during the progression of liver fibrosis.

IgA binds and neutralizes pathogens to prevent infections at mucosal sites in the body. However, emerging evidence shows that IgA contributes to aggravating inflammation or dismantling antitumor immunity in human liver.[21] Liver IgA+ plasma cells directly suppress cytotoxic T-lymphocyte (CTL) activation in vitro and in vivo, inducing CTL exhaustion.[21] Moreover, IgA-deficient mice exhibited markedly reduced HCC development and tumor burden, and PD-L1 blockage induced HCC regression in non-alcoholic steatohepatitis (NASH)-HCC mouse model, thereby reducing tumor load and significantly decreasing liver IgA+ cell abundance.[21] Moreover, co-stimulation with Fc alpha receptor I (FcαRI or CD89) and TLR enhanced proinflammatory cytokine production through various intrahepatic myeloid cells, including Kupffer cells.[22]

Inflammatory stimuli (interferon and IL-6), oncogenic pathways, such as epidermal growth factor receptor and mitogen-activated protein kinase, and other signaling pathways associated with tissue homeostasis, such as the Hippo pathway all regulate PD-L1 expression.[23] Interestingly, recent studies demonstrate that PD-L1 is preferentially expressed in CD68+ monocytes/macrophages in the TME of HCC.[24] Higher expression levels of PD-L1 has been observed in macrophages than in cancer cells, providing a potential indicator of the response to immunotherapy in HCC, whereas PD-L1+ TAMs from analyzed HCC samples did not exhibit complete M2 polarization.[24]

Importantly, previous studies are yet to describe the effects of intrahepatic IgA complex stimulation on PD-L1+ monocytes/TAMs and their effects on inflamed livers and HCC. Moreover, the efficacy of immune-based treatments is limited in patients with NASH-induced HCC.[25] Immunosuppressive liver IgA+ cells block CTL activity, which promotes HCC development in fibrotic NASH livers,[21] indicating the possible negative roles of intrahepatic IgA complex on the efficacy of immune-based treatments in HCC. Therefore, this study investigated the roles of intrahepatic inflammatory IgA+ monocytes in tumor development and immune-based HCC treatments.

METHODS
Patient samples and clinical information
Patient cohorts, including individuals with various liver diseases, including drug-induced liver injury (DILI, n=19), autoimmune hepatitis (AIH, n=11), chronic hepatitis B (CHB, n=44), chronic hepatitis C (CHC, n=31), NASH and ALD, n=61, and HCC (n=271) were established between January 2018 and January 2021. The inclusion criteria were as follows: (1) consecutive patients with liver diseases (DILI, AIH, CHB, CHC, NASH/ALD, and HCC); (2) sera obtained for analyses when patients were enrolled. Detailed clinical parameters of the enrolled patients (CHB cohort, NASH/ALD cohort, and HCC

cohort) are described in online supplemental table 1. Patients' sera were collected and immediately stored at −70°C. Liver biopsy was performed in some patients with chronic liver diseases or HCC. Paraffin blocks and snap-frozen tissues were stored for further use. During surgical resection or liver transplantation of HCC, tumors and non-tumoral tissues were obtained and frozen at −70°C.[26] Portions of the liver tissue were embedded in paraffin for pathological evaluation and immunohistochemistry. In some patients, surgical or biopsy specimens were digested, and mononuclear cells were analyzed as previously described.[24 27] Patients with HCC were diagnosed following recent guidelines by the American Association for the Study of Liver Diseases and the European Association for the Study of the Liver.[27]

The Cancer Genome Atlas survival analysis

Genomic Data Commons Data Portal (https://portal.gdc.cancer.gov/) was used to download the gene expression profiles of 344 patients with HCC and pathologic stages I, II, and III from the The Cancer Genome Atlas (TCGA)-Liver HCC (LIHC) project.[28] In patients with TCGA-LIHC, each stage was divided into two groups based on the average gene expression of immunoglobulin heavy constant alpha 1.[28] They were compared with the overall survival distributions of these patient groups using the log-rank test and Kaplan-Meier curve analysis.

In vitro macrophage polarization, M2 differentiation, and coated IgA stimulation

M2 macrophage polarization was performed as previously described.[24] Human CD14+ monocytes were plated in 90×20 mm cell culture dishes (SPL Life Sciences, Pochon, Korea) containing at 10% Roswell Park Memorial Institute 1640 medium at a density of $1×10^6$ cells/mL. In subsequent days, the medium was supplemented with 1 µg/mL macrophage colony-stimulating factor (M-CSF). Exactly 6 days after inoculation, fresh medium containing 1 µg/mL interleukin (IL)-4 and 1 µg/mL M-CSF was added and maintained at 37°C for 24 hours under a 5% CO_2 condition. Next, 96-well high-affinity Nunc Maxi-Sorp plates (Thermo Fisher Scientific, Waltham, Massachusetts, USA) were coated with 4 µg/mL dimeric IgA (Nordic-MUbio, Susteren, Netherlands) diluted in phosphate-buffered saline (PBS) overnight at 20°C–25°C. This was proceeded by blocking with PBS containing 10% fetal bovine serum for 1 hour at 37°C, and M2-differentiated cells were incubated for 24 hs in IgA complex-coated plate. To verify M2 macrophage activation IgA complex, differentially expressed gene (DEG) analysis, hierarchical clustering, and gene set enrichment analysis (GSEA) were performed on transcriptome sequencing data from the mock and IgA samples. Detailed information on reagents used in this study is presented in online supplemental table 3.

Single-cell RNA-seq analysis

Single-cell RNA-Seq (scRNA-seq) analysis of three public liver cancer datasets was performed. The three datasets (GSE115469, GSE125449set1, and GSE125449set2) were downloaded from the NCBI Gene Expression Omnibus (GEO) database (https://www.ncbi.nlm.nih.gov/geo/query/acc.cgi?acc=GSE115469, https://www.ncbi.nlm.nih.gov/geo/query/acc.cgi?acc=GSE125449, last accessed on November 20, 2021).[11 29] GSE115469 contained 8439 cells from normal liver tissue of five patients, GSE125449set1 contained 5115 primary liver cancer cells from 12 patients, and GSE125449set2 contained 4831 primary liver cancer cells from seven patients. All datasets were generated from high-throughput sequencing experiments designed by 10X Genomics Single Cell 3' v2 Reagent Kit, and gene expression data were made through the 10X Genomics CellRanger pipeline. Additionally, the SCTransform normalization method and anchor-based data integration pipeline introduced by Seurat V.3.1 integrated the three different datasets. After the procedure, various data mining techniques were applied, including dimensionality reduction, clustering algorithms, and statistical tests to discover the relationships between monocytes, T cells, and IgA expression levels in plasma cells. Principal component analysis and uniform manifold approximation and projection (UMAP) methods were sequentially applied to reduce the number of dimensions and to visualize the distributions of cell types via scatter plots. Cell clusters were annotated based on known cell lineage-specific marker genes as previously described.[30] The graph-based clustering algorithm implemented in Seurat was used to distinguish cell types. The DEG analysis was conducted by Welch's t-test and Bonferroni's correction. The data mining pipeline was then implemented using R (V.4.1) and Python (V.3.8) software.

In vivo mouse model

In vivo mice models were generated following a previously described procedure.[31] First, the flanks of 6-week-old C57BL/6N mice were injected with Hepa1-6 cells ($1×10^7$) to obtain HCC syngeneic mouse models. Thereafter, the mice were injected with 100 µg anti-PD-L1 antibody or mock antibody (Bio X Cell, Lebanon, NH, USA), 100 µg FCAR (FcαR) blocking peptides or mock peptides (MyBioSource, San Diego, CA, USA),[32] and 100 mg/kg YAP inhibitor (Verteporfin) or mock inhibitor, following the time regimens. Tumor dimensions were measured using a digital caliper, and volume was calculated as $DW^2/2$ (D, depth; W, width). Mouse tumor tissues and spleens were excised and digested as previously described.[31] Next, the suspension was centrifuged, the supernatant discarded, and the pellets were treated with red blood cell lysis buffer for 5 min at 24°C. Thereafter, the mixture was centrifuged for 5 min at 500×g, washed, the supernatant was discarded, and the pellet was suspended in 100 µL 1×PBS. Finally, fluorescence staining (CD3, CD4, CD8a, CD11b, F4/80, CD45, Ly6G, PD-1, PD-L1, and LIVE/DEAD dye) and fluorescence-activated cell sorting analysis were performed (approval no. CUMS-2020-0301-02).
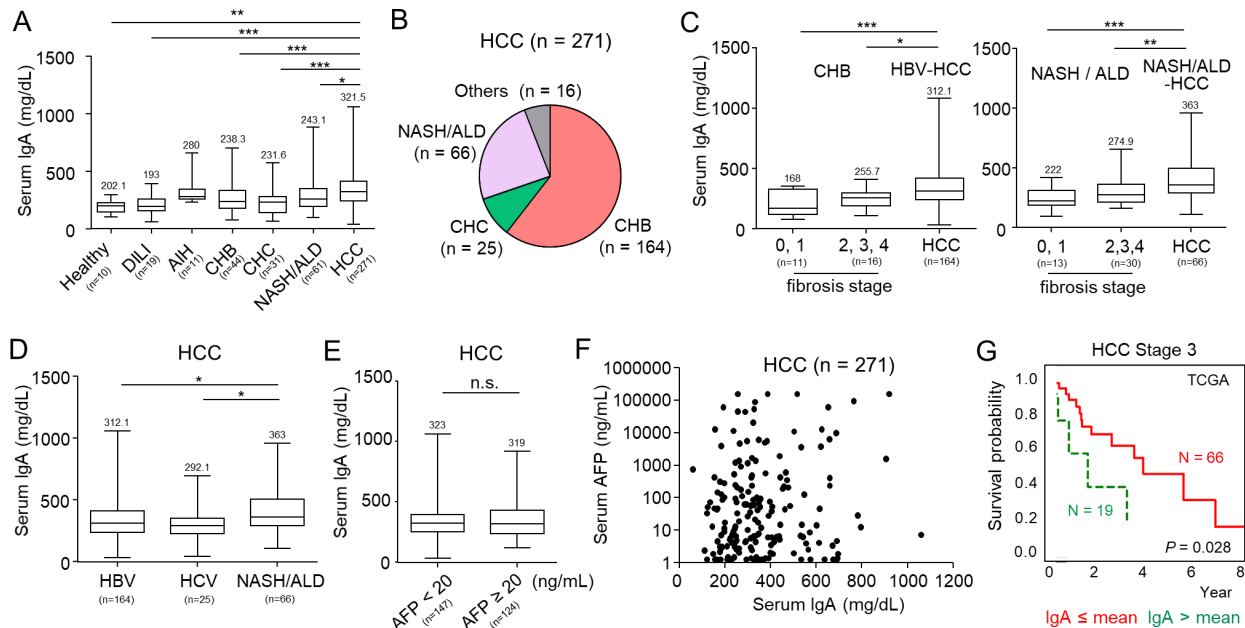
Figure 1 Serum IgA levels correlate with fibrosis progression and HCC development in patients with chronic liver diseases. (A) Higher serum IgA levels in HCC compared with other chronic liver diseases (healthy: n=10, drug-induced liver injury (DILI), n=19, autoimmune hepatitis (AIH): n=11, chronic hepatitis B (CHB): n=44, chronic hepatitis C (CHC): n=31, non-alcoholic steatohepatitis (NASH) and alcoholic liver disease (ALD): n=61, HCC: n=271). (B) Etiologies of HCC patients enrolled in this study (CHB, CHC, NASH/ALD, and others). (C) Serum IgA levels of CHB and HBV-induced HCC and NASH/ALD and NASH/ALD-induced HCC patients. Patients without HCC were classified into 'fibrosis stage 0 and 1' and 'fibrosis stage 2,3, and 4' according to the fibrosis stage. (D) IgA levels in HBV, HCV, and NASH/ALD-induced HCC. (E) Serum IgA levels among patients with HCC and different AFP levels. (F) No correlation between AFP levels and serum IgA levels in patients with HCC. Pearson's correlation analysis was performed. (G) Survival analysis according to intrahepatic IgA transcript level in patients with HCC stage 3 (from TCGA dataset). Continuous variables were assessed using independent t-tests (A–E). For all dataset, median value of each column is presented above the column. *p<0.05, **p<0.01, ***p<0.001. AFP, alpha-fetoprotein; HCC, hepatocellular carcinoma; TCGA, The Cancer Genome Atlas.

Statistical analysis

All statistical analyses were performed using GraphPad Prism V.7 (GraphPad Software, San Diego, California, USA) and SPSS V.24 (IBM SPSS) software or Statistical Package for the Social Sciences (SPSS, V.24.0). Continuous variables were assessed using independent t-tests, whereas the relationships between two parameters were examined using Pearson correlation tests. Wilcoxon matched paired t-test was used to compare data between two paired groups, while Mann-Whitney U test was used for two unpaired groups. Significance between multiple treatment groups was determined using one-way analysis of variance analysis. Means were considered significantly different at p<0.05.

RESULTS
Serum IgA levels correlated with fibrosis progression and HCC development in patients with chronic liver diseases

In this study, the serum IgA levels of patients with various chronic liver diseases were examined (figure 1A). The results showed that patients with HCC had significantly higher serum IgA levels (mean 350.1 mg/dL, median 321.6 mg/dL) than patients with other chronic liver diseases or healthy individuals (figure 1A). The causes of HCC were CHB (60.5%), CHC (9.2%), NASH/ALD

(24.4%), and the other causes (5.9%) (figure 1B). Additionally, we examined the relationship between serum IgA levels and fibrosis progression (F0 and F1 vs F2, F3, and F4) among patients with chronic liver diseases and in liver biopsy samples. Serum IgA levels increased with the progression of fibrosis in patients with liver pathology, although the IgA levels of patients with advanced fibrosis were still significantly lower than those with HCC (figure 1C). This pattern was observed when only patients with CHB and HBV-induced HCC figure 1C or NASH/ALD and NASH/ALD-induced HCC were included (figure 1C). A comparison of serum IgA levels according to HCC etiology showed that patients with NASH/ALD-driven HCC (n=66) exhibited significantly higher serum IgA levels than patients with HBV-driven HCC (n=164) or HCV-driven HCC (n=20) (figure 1D).

The was no significant difference in serum IgA levels between HCC patients with low serum AFP (<20 ng/dL) and those with high serum AFP (≥20 ng/dL) (figure 1E). Additionally, there was no correlation between serum AFP and IgA levels in patients with HCC (figure 1F). Morever there was no significant difference in serum IgA levels between HCC patients with Child-Pugh class A liver function and those with Child-Pugh class B liver function (online supplemental figure 1A). Serum IgA levels were

not associated with tumor staging or portal vein tumor thrombosis (data not shown). Based on TCGA dataset, we found that among patients with HCC stage 3, an intrahepatic IgA transcript level below the mean level was associated with a significantly higher survival probability (figure 1G). This association was not observed among the earlier staged tumors (online supplemental figure 1B).

IgA⁺ monocytes are enriched and show high levels of PD-L1 in NASH/ALD livers

CD89 (FcαRI) expression levels were extremely low in T cells, but significantly higher in CD14⁺ cells and B cells in healthy human liver (figure 2A). The surface expression level of CD89 in intrahepatic CD14⁺ monocytes from NASH/ALD livers was significantly higher than that from healthy livers (figure 2B). Using peripheral blood mononuclear cells (PBMCs) from a healthy donor, we investigated whether IgA complex binds to CD89 on the immune cell surface. A higher number of IgA dimers was bound to CD14⁺ monocytes than to CD3⁺ T cells in the presence of Pam3csk4 (Pam3CysSerLys4, TLR2/TLR1 ligand) (figure 2C). Immunohistochemistry confirmed the expression of CD3, CD68, and IgA in healthy liver and NASH-induced cirrhotic liver (figure 2D). IgA positivity was mainly observed in sinusoidal endothelial and Kupffer cells in healthy liver. In NASH-induced cirrhotic liver, CD3⁺ and CD68⁺ cells were observed in the expanded portal tract, and IgA⁺ cells were mainly located in the portal tract and fibrotic bands. IgA staining was strongest in some plasma cells (online supplemental figure 2A) and in monocytes/Kupffer and endothelial cells in NASH-induced cirrhotic liver (online supplemental figure 2B); however, IgA was barely detected in hepatocytes (online supplemental figure 2A,B).

Interestingly, the number of CD68⁺ (figure 2E) and IgA⁺ cells (figure 2F) increased with the progression of fibrosis in NASH/ALD livers. Moreover, there was a strong positive correlation between serum IgA levels and the number of intrahepatic IgA⁺ cells in NASH/ALD livers (figure 2G). To detect TLR agonist in NASH liver tissue, we performed immunohistochemistry for TLR4 and LPS, and found that LPS⁺ and TLR4⁺ cells were highly detected in NASH-cirrhotic liver (online supplemental figure 3). Additionally, several Kupffer cells/monocytes showed positivity for LPS (online supplemental figure 3A) and TLR4 staining (online supplemental figure 3B) in NASH-cirrhotic livers. Furthermore, we performed IHC for IgA in the same samples. Overall, when the liver tissue shows strong positivity to IgA staining, TLR4 and LPS staining were also strong, suggesting that IgA complex binding and internalization may be tightly associated with TLR and its ligand binding in intrahepatic monocytes (online supplemental figure 3C).

A representative gating strategy for intrahepatic monocytes is presented in figure 2H (data from a patient with cirrhotic NASH). Traditionally, monocytes are classified into three subgroups according to their CD14 and CD16 expression status: classical, intermediate, and non-classical

monocytes.[33] Intrahepatic CD14⁺ monocytes with high IgA levels showed PD-L1 positivity in cirrhotic NASH liver (figure 2I). Additionally, correlation analysis showed that the frequency of intrahepatic IgA⁺ CD14⁺ monocytes was positively correlated with the frequencies of PD-L1⁺ cells in NASH/ALD patients (n=20) (figure 2J). CD163 expression level was used as a potential marker of immune-regulatory cells (including Kupffer cells) as previously described.[20] A comparison of IgA levels between intrahepatic CD163^high and CD163^low monocytes in NASH/ALD livers (n=13) showed that there was no significant difference in the frequency of IgA⁺ cells between the two groups (figure 2K).

Furthermore, in vivo experiments were performed using various animal models to confirm our findings. First, we established acute and chronic hepatitis mouse models using Con A injection with different doses and schedules (online supplemental figure 4A). There was a marked increase in alanine aminotransferase (ALT) levels in the acute hepatitis model, whereas the chronic hepatitis model showed a slight increase in ALT compared with mock-treated mice (online supplemental figure 4B). Additionally, intrahepatic immune cells were analyzed by multicolor flow cytometry. In both the acute and chronic hepatitis models, we observed significantly increased numbers (per g liver weight) of intrahepatic CD11b⁺F4/80⁺ macrophages, PD-L1⁺CD11b⁺F4/80⁺ macrophages (online supplemental figure 4C), intrahepatic IgA⁺ cells, and IgA⁺PD-L1⁺CD11b⁺F4/80⁺ macrophages (online supplemental figure 4D). These increments were more pronounced in the chronic hepatitis model.

IgA⁺ monocytes show high levels of PD-L1 in HCC TME

Furthermore, we investigated the expression and phenotypes of IgA⁺ intrahepatic monocytes in HCC tumor tissues. Immunohistochemical staining demonstrated infiltration of CD3⁺ T cells, CD38⁺ plasma cells, and CD68⁺ macrophages in HCC TME (figure 3A). IgA was strongly expressed in some cells, showing positive staining for CD38. Additionally, other non-parenchymal cells, including CD68⁺ cells, showed positive staining for IgA (figure 3A). Among HCC patients with IgA immunohistochemical staining results (n=65), serum IgA levels were positively correlated with total IgA⁺ cell infiltration in HCC TME (figure 3B).

Additionally, cell surface markers of monocytes in digested tumor tissues and distant non-tumor tissues of HCC patients were analyzed. Figure 3C presents representative flow cytometry data of a patient with high serum IgA. Intrahepatic monocyte subgroups showed different distribution patterns in intratumoral/peritumoral regions and distant non-tumor regions. Several monocytes in both intratumoral/peritumoral and distant non-tumor regions showed IgA positivity in patients with high serum IgA levels (figure 3C). Additionally, IgA⁺ monocytes were highly positive for PD-L1 staining compared with IgA⁻ monocytes in these patients (figure 3C).
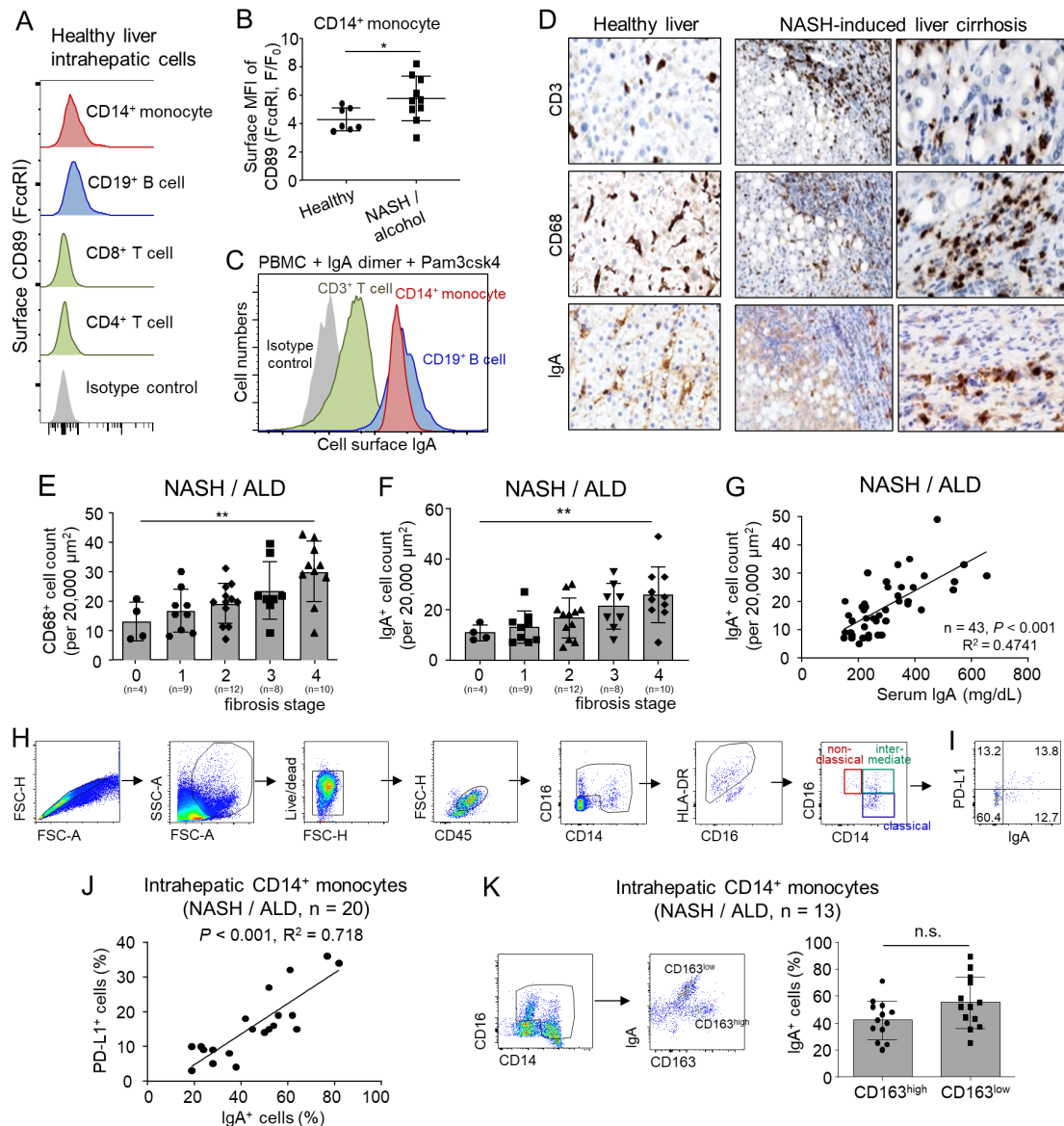
Figure 2 IgA+ Monocytes are enriched and show high levels of PD-L1/HLA-DR in NASH/ALD livers. (A) CD89 (FcαRI) expression in various intrahepatic immune cells from a healthy liver. Representative flow cytometry data from five independent liver samples. (B) Surface MFI of CD89 in CD14+ monocytes from healthy (n=7) and NASH/alcohol livers (n=10). (C) Surface IgA staining results after incubation of PBMC with IgA dimer and Pam3csk4 (Pam3CysSerLys4, TLR2/TLR1 ligand) for 1 hour. Vigorous washing was performed before IgA detection. The amount of IgA bound to the immune cell surface is presented as a histogram. Representative data from three independent experiments. (D) Representative immunohistochemistry results for CD3, CD68, and IgA expression in a healthy liver and NASH-induced cirrhotic liver. (E) The number of intrahepatic CD68+ cells according to liver fibrosis stage in patients with NASH/ALD (F0: n=4, F1, n=9, F2: n=12, F3: n=8, F4: n=10). **P<0.01. (F) The number of intrahepatic IgA+ cells according to liver fibrosis stage in patients with NASH/ALD (F0: n=4, F1, n=9, F2: n=12, F3: n=8, F4: n=10). *P<0.05. (G) Correlation between serum IgA level and IgA+ cell number in NASH/ALD livers (n=43). Pearson's correlation analysis was performed. (H) Gating strategy for intrahepatic monocyte populations (NASH patient). (I) The representative dot-plot describes the proportions of IgA+ and PD-L1+ cells in NASH-induced cirrhotic liver. (J) IgA and PD-L1 positivity was analyzed in CD14+ monocytes by flow cytometry. Association between IgA+ cells and PD-L1+ cells among intrahepatic CD14+ monocytes in patients with NASH/ALD is presented (n=20). Pearson's correlation analysis was performed. (K) Frequency of IgA+ cells between intrahepatic CD163high and CD163low monocytes in NASH/ALD livers (n=13). Continuous variables were assessed using independent t-tests (B, K). One-way ANOVA analyses were used when performing multiple comparisons (E, F). ALD, alcoholic liver disease; ANOVA, analysis of variance; MFI, mean fluorescence intensity; NASH, non-alcoholic steatohepatitis; n.s., not significant; PBMC, peripheral blood mononuclear cell.

However, circulating CD14+ monocytes showed extremely low positivity for IgA and PD-L1 staining (figure 3D). IgA+ cells exhibited significantly higher frequency among intratumoral/peritumoral CD14+ monocytes than among circulating monocytes (figure 3E). In HCC patients with high serum IgA, intratumoral/peritumoral monocytes tended to show higher IgA and PD-L1 levels than distant non-tumoral monocytes (figure 3F). However, this was not
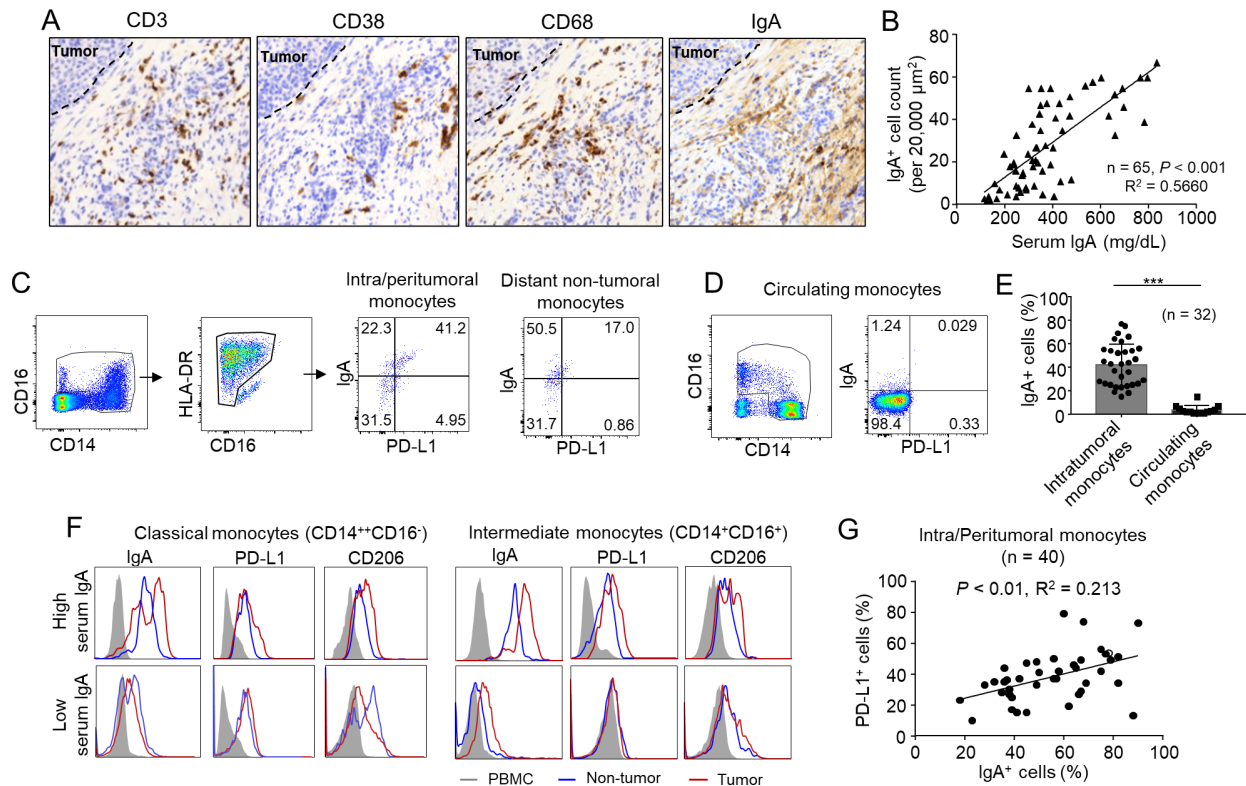
Figure 3 IgA+ monocytes show high PD-L1/HLA-DR levels in HCC tumor microenvironment. (A) Representative findings of immunohistochemical staining for CD3, CD38, CD68, and IgA expressions in HCC TME. (B) Correlation between serum IgA levels and IgA+ cell number in HCC TME (n=65). Pearson's correlation analysis was performed. (C, D) Representative dot-plot describes the proportions of IgA+ and PD-L1+ cells among intratumoral/peritumoral CD14+ monocytes, distant non-tumor CD14+ monocytes, and circulating CD14+ monocytes in HCC patient with high serum IgA. (E) Frequency of IgA+ cells in the TME and peripheral blood in HCC patients (n=32). Independent t-test was used. ***p<0.001. (F) Representative histogram of the frequencies of IgA+, PD-L1+, and CD206+ cells among classical monocytes and intermediate monocytes in patients with high and low serum IgA. (G) Association between the numbers of IgA+ cells and PD-L1+ cells among intratumoral/peritumoral CD14+ monocytes analyzed by flow cytometry (n=40). Pearson's correlation analysis was performed. HCC, hepatocellular carcinoma; TME, tumor microenvironment.

the case in patients with low serum IgA. Correlation analysis showed that there was a positive correlation between intratumoral/peritumoral IgA+CD14+ monocytes and the frequencies of PD-L1+ cells in the TME of HCC (n=40) (figure 3G).

scRNA sequencing data from GEO database reveal that livers with higher levels of IgA-producing plasma cells are enriched with monocytes with inflammatory phenotypes

The three datasets (GSE115469, GSE125449set1, and GSE125449set2) were downloaded from the NCBI GEO database for scRNA-seq analysis. The UMAP analysis, which was performed as previously described,[34] demonstrated eight cell lineages (online supplemental figure 5A). To better delineate subpopulations of each cell type, all cells were further classified into 30 clusters as previously described (online supplemental figure 5A,B).[30 35] Markers, such as *IGHA1* and *IGHG1,* were highly expressed in plasma cell lineage (figure 4A). Among 24 tissues analyzed (5 healthy livers and 19 tumors), plasma cells were detected in 18 tissues. The average expression level of IgA (IGHA1 gene) in plasma cells was computed for each tissue, and the median *IGHA1* expression was 1.245

(figure 4B and online supplemental table 2). Plasma cell IGHA1 expression was higher in some HCC patients than in others and healthy controls. However, the expression level was not significantly different between HCC patients and healthy controls (figure 4B).

Clusters 6, 12, and 20 were annotated as 'monocytes in the previous report.'[30] The expression of *CD14, CD16, CD86, CD54,* and *HLA-DRA* in each cluster is presented in online supplemental figure 5C. From cluster 12, cells derived from the 18 patients were collected, and 286 significant DEGs (adjusted p<0.01) were identified in monocytes between patients whose plasma cell IgA expression was greater than or equal to median vs those whose plasma cell IgA expression was less than the median. Additionally, *LYZ, AREG, KLF6, FOSB, CLEC9A,* and *SAA*2, which are well-known genes associated with the activation pathways of monocytes, were significantly upregulated in cluster 12 lineage of patients whose plasma cell IgA expression was greater than or equal to the median (figure 4C).

Regarding T cells, we used markers described in a previous report,[35] in which T cells were divided into
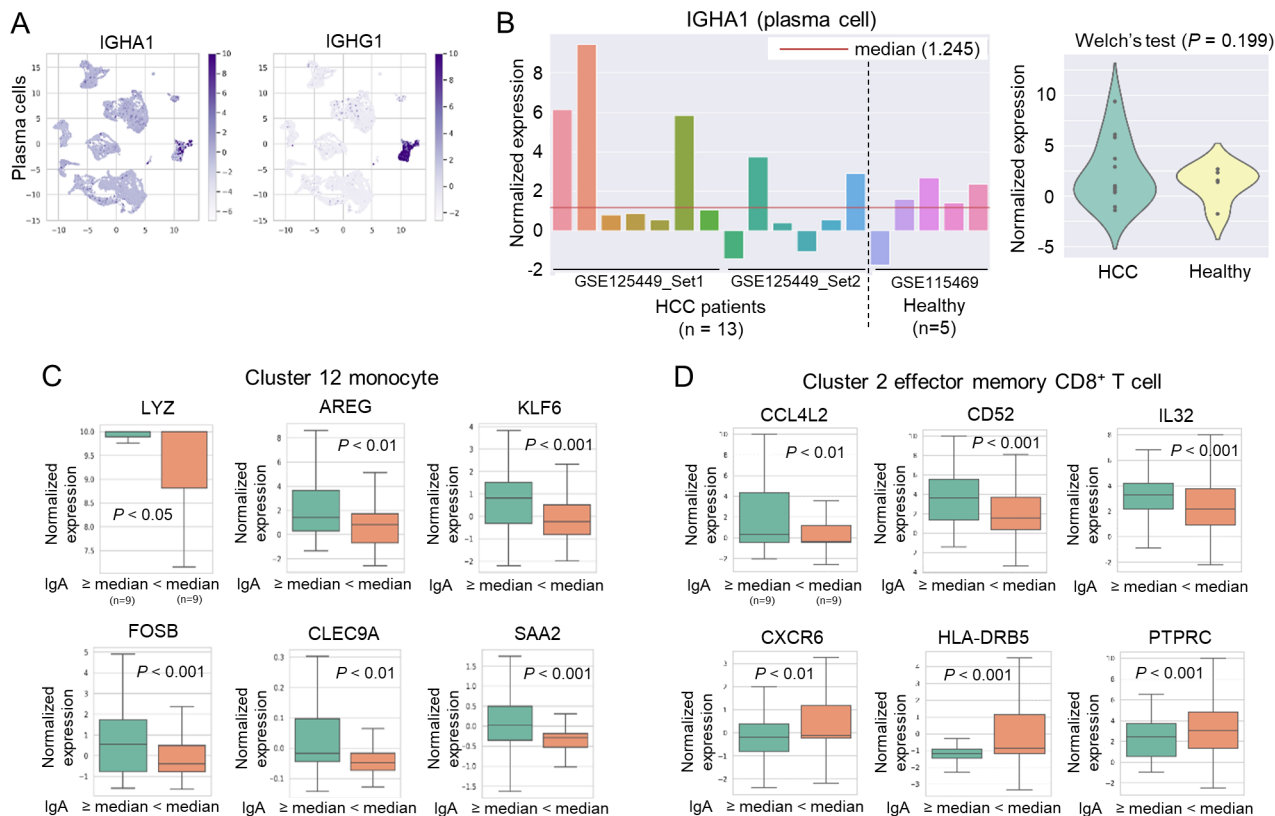
Figure 4 scRNA sequencing reveals that livers with high IgA-producing plasma cell are enriched with monocytes with inflammatory phenotypes. (A) Identification of plasma cells using known markers as previously described.[30] (B) The average expression level of IgA (*IGHA1* gene) in plasma cells in 18 tissues. *IGHA1* gene expression levels in plasma cells were compared between HCC tissues and healthy livers. (C) Expression of genes associated with inflammation (*LYZ, AREG, KLF6, FOSB, CLEC9A*, and *SAA2*) in cluster 12 lineage between patients whose plasma cell IgA expression was greater than or equal to median and those whose plasma cell IgA expression was less than the median. (D) Expression of genes associated with CD8^{+} T cell activation (*CCL4L2, CD52,* and *IL32*) and immune-regulatory function (*CXCR6, HLA-DR5, PTPRC*) in cluster two lineage between patients whose plasma cell IgA expression was greater than or equal to median and those whose plasma cell IgA expression was less than the median. The DEG analysis was conducted by Welch's *t*-test and Bonferroni's correction. DEG, differentially expressed gene; HCC, hepatocellular carcinoma.

11 categories, including effector memory CD8^{+} T cells and exhausted CD8^{+} T cells. Using the six markers mentioned in that report (*FCGR3A, FGFBP2, CTLA4, PDCD1, HAVCR2, GZMK*), we identified T cell subtypes in our clusters. Cluster 2 showed 'effector memory' CD8^{+} T cell phenotype, whereas cluster 24 showed 'exhausted' CD8^{+} T cell phenotype (online supplemental figure 5D). Interestingly, *CCL4L2, CD52,* and *IL32*, which are well-known genes associated with the activation pathways of T cells, were significantly upregulated in cluster 2 lineage of patients whose plasma cell IgA expression was greater than or equal to the median. In contrast, immune-regulatory genes (*CXCR6, HLA-DR5, PTPRC*) were significantly downregulated in these individuals (figure 4D).
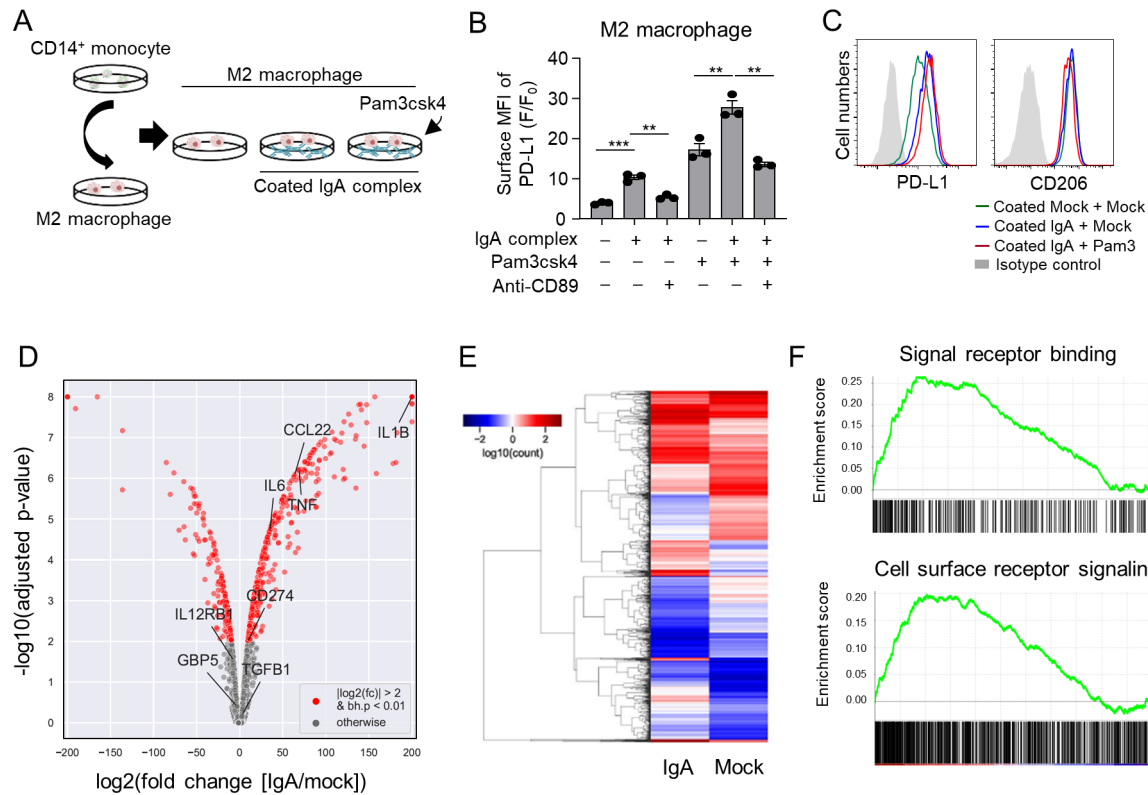
In vitro stimulation of M2 macrophages with coated IgA complex induces intracellular signaling cascade resulting in upregulation of cell surface PD-L1

To determine the effects of IgA complex stimulation of macrophages, M2 macrophages were differentiated from peripheral monocytes and stimulated with coated IgA dimer derived from human sera, with or without Pam3csk4

(figure 5A). After 24 hours of stimulation with coated IgA complex, there was an upregulation in PD-L1 expression, which was more obvious after costimulation with Pam3csk4 (figure 5B). Blocking CD89 with the specific antibody stopped IgA complex-mediated PD-L1 upregulation (figure 5B). However, CD206 expression was not affected by coated IgA stimulation (figure 5C). The same experiments were performed using M1-differentiated macrophages, and similar results were obtained (data not shown).

Next, RNA sequencing was performed after stimulation of M2 macrophages with mock or coated IgA complex. The results of DEG analysis are presented in a volcano plot (figure 5D). Genes that were upregulated after macrophage activation (*IL1B, CCL22, TNF*, and *IL6*) were significantly upregulated after coated IgA stimulation of M2 macrophages (figure 5D). Hierarchical clustering revealed overall differences in gene expression patterns between the mock-treated and coated IgA-treated macrophages (figure 5E). GSEA showed activation of receptor-mediated signaling pathways after coated IgA stimulation of M2 macrophages (figure 5F).

Figure 5 In vitro stimulation of M2 macrophages with coated IgA complex induces a signaling cascade resulting in the activation and upregulation of cell surface PD-L1. (A) Experimental scheme of M2 macrophage differentiation from peripheral monocytes and their stimulation with coated IgA complex derived from human sera. (B, C) PD-L1, not CD206, was upregulated after M2 macrophage stimulation with coated IgA complex ±Pam3csk4 (Pam3) for 24 hours. Macrophages were pretreated with CD89 blocking antibody or mock antibody 1 hour before incubating cells in IgA-coated culture well. Independent t-test was used. **P<0.01, ***p<0.001. Five replicates of the experiments with the same protocol were performed. (D, E) RNA sequencing data after M2 macrophage stimulation with mock or coated IgA complex. The results of DEG analysis are shown in a volcano plot (D), hierarchical clustering (E), and GSEA (F). DEG, differentially expressed gene; GSEA, gene set enrichment analysis; MFI, mean fluorescence intensity.
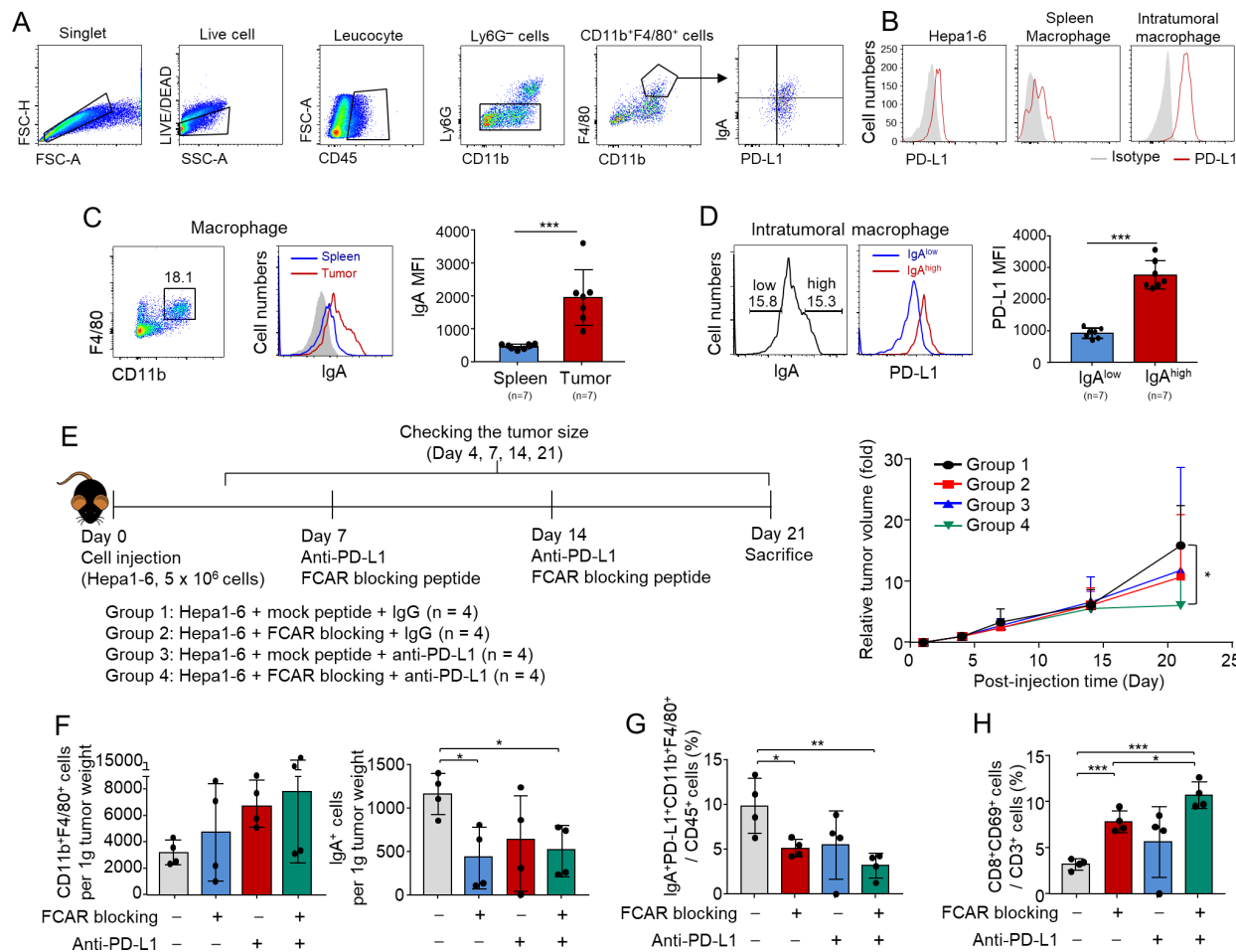
Neutralization of IgA in syngeneic HCC mouse model causes depletion of intratumoral IgA+ macrophages and infiltration of intratumoral CD69+CD8+ T cells

To confirm the roles of IgA+ macrophages in the TME, syngeneic HCC mice models were generated. The representative gating strategy of intratumoral macrophages is presented in figure 6A. A previous study demonstrated preferential PD-L1 expression in macrophages compared with tumor cells in syngeneic HCC mouse model and patient HCC tissues.[24] Similarly, the results of this study confirmed high PD-L1 expression in intratumoral macrophages (figure 6B). As expected, intratumoral macrophages had higher IgA levels than spleen macrophages (figure 6C), and PD-L1 levels were higher in intratumoral IgA^high macrophages than intratumoral IgA^low macrophages (figure 6D). Furthermore, we used FCAR-blocking peptides to neutralize secreted IgA complex, and anti-PD-L1 antibody to block PD-L1 molecules on the surface of macrophages (figure 6E). Intraperitoneal injection of FCAR-blocking peptide only or anti-PD-L1 did not significantly reduce tumor volume when 5×10^6 cells were initially injected. However, combined FCAR-blocking peptide and anti-PD-L1 treatment caused a decrease in tumor volume

(figure 6E). Moreover, FCAR-blocking peptide treatment caused a decrease in intratumoral IgA+ cell population (figure 6F), although there was no significant change in the number of intratumoral CD11b+ F4/80+ macrophages (figure 6F). FCAR-blocking peptide treatment also caused a decrease in the frequencies of IgA+PD-L1+ macrophages (figure 6G). The number of intratumoral CD69+CD8+ T cells increased after treatment with FCAR-blocking peptide and further increased after cotreatment with FCAR-blocking peptide and anti-PD-L1 antibody (figure 6H).

In vitro and in vivo blockage of YAP/TAZ signaling decreases cell surface PD-L1 expression in intratumoral IgA+ macrophages

To investigate the putative mechanisms of how IgA complex activates macrophages and upregulates PD-L1 in these cells, we performed in vitro experiments using M2 macrophages differentiated from peripheral monocytes. We pretreated M2 macrophages with various chemical inhibitors before treatment with coated IgA complex. Among the inhibitors examined, only YAP inhibitor suppressed coated IgA complex-induced upregulation

Figure 6 IgA neutralization in a syngeneic HCC mouse model causes a decrease in intratumoral IgA$^+$ macrophages and infiltration of intratumoral CD69$^+$CD8$^+$ T cells. (A) Gating strategy of intratumoral CD11b$^+$F4/80$^+$ macrophages in a syngeneic mouse tumor. (B) Cell surface PD-L1 levels in Hepa1-6 cells and macrophages. (C) Comparative analysis of surface IgA levels in intratumoral and splenic macrophages. (D) Comparative analysis of PD-L1 levels in IgA^{high} and IgA^{low} intratumoral macrophages. (E) Syngeneic HCC mouse model (5×10^6 cells) using FACR-blocking peptide and/or anti-PD-L1 antibody. Serial changes in the sizes of tumors generated from Hepa1-6 cells (5×10^6 cells) after FACR-blocking peptide and/or anti-PD-L1 antibody administration. (F) Numbers of intratumoral CD11b$^+$F4/80$^+$ cells and IgA$^+$ cells per 1 g tumor weight in syngeneic HCC mouse model. (G) Number of intratumoral IgA$^+$CD11b$^+$F4/80$^+$ cells per CD45$^+$ cells in the syngeneic HCC mouse model. (H) Number of intratumoral CD69$^+$CD8$^+$ T cells per CD3$^+$ cells in the syngeneic HCC mouse model. Continuous variables were assessed using independent t-tests (C–G). *P<0.05, **p<0.01, ***p<0.001. HCC, hepatocellular carcinoma; MFI, mean fluorescence intensity.

of PD-L1 level (figure 7A). Moreover, adding Pam3csk4 to IgA complex-stimulated M2 macrophages further increased PD-L1 upregulation, which was inhibited by YAP inhibitor (figure 7A). Similarly, YAP inhibitor inhibited IgA complex-mediated upregulation of IL-1β and IL-10 (figure 7B). Immunoblotting with subcellular fractionation revealed that the YAP molecule translocated into the nuclei after IgA complex stimulation of M2 macrophages (figure 7C).

Next, we performed in vivo experiments using a mouse model (1×10^6 Hepa1-6 cells) to evaluate the effects of YAP inhibitors on intratumoral IgA$^+$ macrophages. Four groups were established with either YAP inhibitor or anti-PD-L1 treatment or both (figure 7D). YAP inhibitor alone did not significantly reduce tumor size, but anti-PD-L1 treatment or anti-PD-L1 plus YAP inhibitor treatment caused a considerable decrease in tumor size, although

the decrease was evident 21 days after injection of tumor cells (figure 7D). Additionally, YAP inhibitor did not significantly affect the number of infiltrated IgA$^+$ cells or macrophages in 1 g syngeneic tumor weight (figure 7E). However, the frequency of PD-L1$^+$ macrophages was lower in the YAP inhibitor-treated group than in the mock-treated group (figure 7F). Moreover, YAP inhibitor treatment decreased the mean fluorescence intensity of PD-L1 in IgA$^+$PD-L1$^+$ intratumoral macrophages (figure 7G).

DISCUSSION

The results of this study showed that there was an increase in serum IgA levels in HCC patients, which was correlated with intrahepatic or intratumoral infiltration of inflammatory IgA$^+$PD-L1^{high} monocytes/macrophages. Additionally, it was observed that IgA neutralization and anti-PD-L1
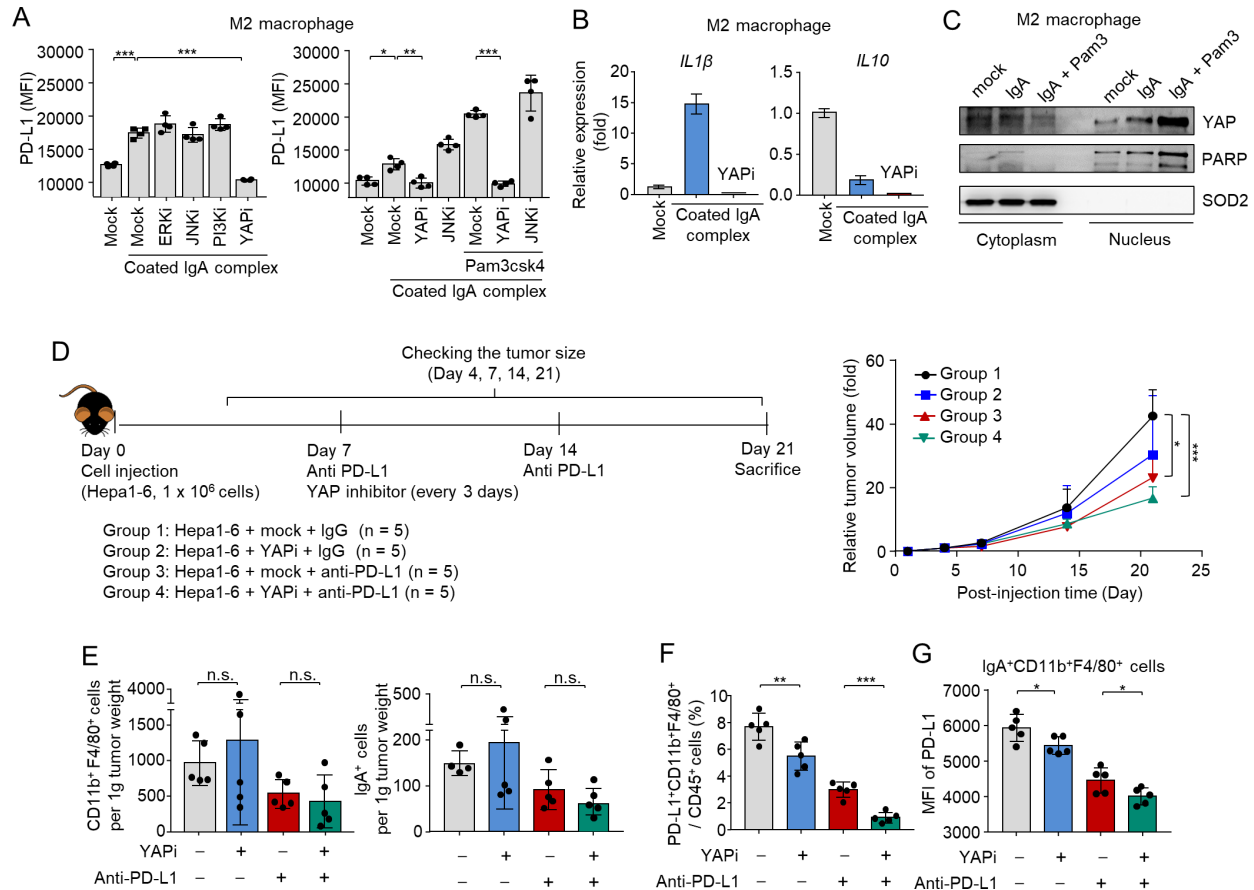
Figure 7 In vitro and in vivo YAP/TAZ signaling blockade decreases cell surface PD-L1 expression in intratumoral IgA+ macrophages. (A) M2 macrophages were treated with various chemical inhibitors 12 hours before treatment with coated IgA complex and/or Pam3csk4 (Pam3), and cell surface PD-L1 expression was measured. *P<0.05, **p<0.01, ***p<0.001. (B) RT-qPCR data for IL-10 and IL-1β after stimulation of M2 macrophages with coated IgA complex with or without YAP inhibitor. Data are representative of five independent experiments. (C) Representative immunoblotting data after subcellular fractionation for YAP, PARP, and SOD2 after stimulation of M2 macrophages with coated IgA complex and/or Pam3. Data are representative of three independent experiments. (D) Experiment schedule in the syngeneic HCC mouse model (1×10⁶ cells) using YAP inhibitor and/or anti-PD-L1 antibody. Serial changes in the size of tumors generated from Hepa1-6 cells (1×10⁶ cells) after YAP inhibitor and/or anti-PD-L1 antibody. (E) Numbers of intratumoral CD11b+ F4/80+ cells or IgA+ cells per 1 g tumor weight in the syngeneic HCC mouse model. (F) Numbers of intratumoral PD-L1+ CD11b+ F4/80+ cells per CD45+ cells in the syngeneic HCC mouse model. (G) MFI of PD-L1 in IgA+CD11b+ F4/80+ cells after treatment with YAP inhibitor and/or anti-PD-L1 antibody. Continuous variables were assessed using independent t-tests (A, D–G). *P<0.05, **p<0.01, ***p<0.001. HCC, hepatocellular carcinoma; MFI, mean fluorescence intensity; n.s, not significant.

target these cells, indicating that inflammation-induced IgA complex in the liver play a critical role in HCC development in chronic liver diseases. Furthermore, IgA complex-stimulated monocytes/macrophages expressed higher PD-L1 levels in HCC TME, indicating that these cells could possibly be target during HCC treatment to enhance the efficacy of immune-based therapy. Moreover, IgA+PD-L1^high monocytes showed activated phenotypes in scRNA-seq, suggesting that the cells can stimulate intrahepatic CD8+ T cells and simultaneously cause PD-L1-mediated T cell dysfunction.

Macrophages in the liver include immune-regulatory Kupffer cells, which are tissue-localized and capable of self-renewal. Within HCC TME, mononuclear phagocytes (TAMs) develop primarily from MoMFs, rather than Kupffer cells.[36] TAMs support tumor angiogenesis, invasion, growth, and metastasis. A recent study developed a myeloid-specific prognostic signature, referred to as the myeloid response score (MRS) for HCC.[37] A high MRS is associated with a strong protumoral activity in the TME and poor survival outcomes.[37] Moreover, recent studies demonstrated that HCC TME is infiltrated by PD-L1+ activated monocytes with protumoral features.[14 15] Hence, HCC can be prevented or managed by targeting TAM functions in the TME. A previous study showed that PD-L1 is preferentially expressed in macrophages instead of in cancer cells, potentially serving as an immunotherapy-predicting factor in HCC. Additionally, it was observed that PD-L1+ TAMs from the analyzed HCC samples did not exhibit complete M2 polarization.[24] Moreover, these TAMs showed high HLA-DR expression, which reflects the potential immunogenic nature and susceptibility of tumor cells to therapy designed to decrease the proliferation of PD-L1-expressing TAMs.[10]

Previous studies have reported high serum IgA levels in patients with NASH and ALD, which increased according to fibrosis score[38 39]; however, the roles of accumulated intrahepatic IgA in HCC are yet to be elucidated. In the liver of patients with NAFLD or chronic inflammation from other etiologies, damage-associated molecular patterns or endotoxins stimulated macrophages via TLR molecules, and secreted IgA complex can stimulate macrophages cooperatively with TLR molecules.[22] Additionally, the immunosuppressive function of IgA+ plasma cells to disrupt CTL activation has been demonstrated in a previous study.[40] A subsequent study showed that CTL activation was inhibited by hepatic IgA+ plasma cells both in vitro and in vivo.[21] In major urinary protein-urokinase-type plasminogen activator mice, HCC regressed after PD-L1 inhibition, decreasing tumor burden and markedly reducing the number of hepatic IgA+ plasma cells.[21] In this study, we elucidated the roles of IgA complex in intrahepatic monocytes/macrophages and the potential mechanisms of IgA complex-induced PD-L1 upregulation in stimulated cells. Additionally, treatment with soluble FCAR-binding peptide and anti-PD-L1 antibody caused a decrease in IgA+ monocytes population in HCC mice models. In patients with chronic liver diseases, there is an accumulation of inflammatory IgA+ monocytes expressing PD-L1 in the precancerous liver. Although previous studies focused mainly on the possible roles of IgA+ plasma cells, this study focused on IgA+ monocytes in both animal models and diseased human livers and HCC tissues.

One thing to consider is that differences of the tumor volumes shown in the different groups emerged only after day 21 in our mice experiments (figures 6E and 7D). This protracted effect of anti-PD-L1 and FCAR blocking may have occurred because the drugs were not cytotoxic but they are drugs that evoke antitumor immune responses. Even when these drugs are started concomitantly with the injection of the tumor cells, the differences in tumor volumes between groups were only evident after day 21 (online supplemental figure 6). Patients with HCC treated with immune-based therapies may also experience the pseudo-progression, which is defined as an initial increase in tumor burden, followed by tumor shrinkage. While the mechanism of pseudoprogression is not fully understood, tumor necrosis and immune cell infiltration may be responsible for the phenomenon.[41] This initial inflammatory reaction may be the cause of delayed tumor-shrinking effects of anti-PD-L1 and FCAR blocking in our in vivo model.

Recently, nivolumab was approved as second-line therapy for advanced HCC management, and atezolizumab plus bevacizumab was recently shown to be superior to sorafenib as primary treatment for advanced HCC. However, the efficacy of these immune-based treatments was limited in patients with NASH-induced HCC.[25] A recent study demonstrated that NASH limits antitumor surveillance in immunotherapy-treated HCC via the accumulation of hepatic unconventionally activated CD8+PD1+ T cells in NASH livers,[25] although the specific mechanism was not elucidated. However, we speculated that IgA complex-activated PD-L1+ macrophages may be one of the contributing factors for the accumulation of CD8+ T cells. To enhance the efficacy of ICIs in HCC patients, it may be needed to suppress the activity of IgA+ macrophages.

The findings of this study showed that in vitro stimulation of M2-polarized macrophages with the coated IgA complex induced the activation of YAP/TAZ-mediated signaling pathway, resulting in cell activation and PD-L1 upregulation. A recent study has implicated the Hippo signaling pathway as a major target in preventing HCC initiation.[42] A key component of the Hippo pathway is the inhibition of YAP/TAZ transcription factors by the Hippo kinase cascade. Abnormal YAP or TAZ activation has been observed in several human cancers, including HCC.[43] Interestingly, PD-L1 is a target of Hippo signaling, and TAZ-induced PD-L1 upregulation was sufficient to inhibit cytotoxic T-cell function.[43] Several studies have demonstrated YAP involvement in the interactions between tumor and immune cells, particularly TAMs.[44] A previous study revealed that YAP inhibited M2 macrophage polarization and promoted IL-6 production in M1 macrophages in a mouse model with inflammatory bowel diseases.[45] Similarly, the findings of this study indicated that YAP-mediated PD-L1 upregulation may be caused by IgA-mediated stimulation and is accompany the activation of macrophages.

In the in vivo experiments (figure 7D), there was only a marginal (non-significant) difference in tumor volumes between group 3 (anti-PD-L1 only) and group 4 (YAPi+anti-PD-L1). Through our in vitro and in vivo experiments, it was confirmed that YAP is critical in PD-L1 upregulation in monocytes/macrophages. However, for the antitumor effects, combined treatment of YAPi and ICIs did not yield superior antitumor effects to ICI monotherapy in our three different sets of in vivo experiments. The reasons for the discrepancy may arise from the fact that YAP/TAZ pathway may function in a protumoral way in some cellular compartments of TME of HCC, and may function in an antitumoral way in some cellular compartments.[46–48] In this study, we only focused on the role of YAP/TAZ in monocytes/macrophages of HCC TME. The detailed role of targeting YAP/TAZ in immune-based therapies for HCC should be further investigated in the future.

This study was limited by the small sample size and availability of human tissue for immunohistochemical analysis and flow cytometry. Additionally, the liver cancer model used in this study was developed via orthotopic method, not spontaneous cancer development. Therefore, further animal studies are required to validate our results using a spontaneous HCC developing mouse model.

CONCLUSION

Overall, the findings of this study indicated that there was an increase in serum IgA levels in HCC patients, which was associated with intrahepatic infiltration of inflammatory IgA$^+$PD-L1^{high} monocytes. Additionally, targeting IgA signaling in chronically inflamed livers may enhance antitumor immune responses by suppressing IgA$^+$ monocytes/macrophages activity. Moreover, IgA$^+$PD-L1^{high} monocytes showed PD-L1 upregulation, which may cause antitumor T cell dysfunction in HCC TME. Therefore, targeting intrahepatic IgA may enhance the efficacy of immune-based therapy.

Author affiliations
^{1}Division of Gastroenterology and Hepatology, Department of Internal Medicine, College of Medicine, Seoul St. Mary's Hospital, The Catholic University of Korea, Seoul, South Korea
^{2}The Catholic University Liver Research Center, College of Medicine, Department of Biomedicine & Health Sciences, The Catholic University of Korea, Seoul, South Korea
^{3}Department of Hospital Pathology, College of Medicine, Eunpyeong St. Mary's Hospital, The Catholic University of Korea, Seoul, South Korea
^{4}Department of Hospital Pathology, College of Medicine, Seoul St. Mary's Hospital, The Catholic University of Korea, Seoul, South Korea
^{5}Division of Gastroenterology and Hepatology, Department of Internal Medicine, College of Medicine, Eunpyeong St. Mary's Hospital, The Catholic University of Korea, Seoul, South Korea
^{6}Department of Computer Science, Yonsei University, Seoul, South Korea
^{7}Department of Computer Science & Engineering, Incheon National University, Incheon, South Korea

ORCID iD
Pil Soo Sung http://orcid.org/0000-0002-4476-4868

REFERENCES

1 European Association for the Study of the Liver. Electronic address eee, European association for the study of the L. EASL clinical practice guidelines: management of hepatocellular carcinoma. *J Hepatol* 2018;69:182–236.
2 Kang F-B, Wang L, Li D, *et al*. Hepatocellular carcinomas promote tumor-associated macrophage M2-polarization via increased B7-H3 expression. *Oncol Rep* 2015;33:274–82.
3 Hilmi M, Neuzillet C, Calderaro J, *et al*. Angiogenesis and immune checkpoint inhibitors as therapies for hepatocellular carcinoma: current knowledge and future research directions. *J Immunother Cancer* 2019;7:333.
4 Lee C-H, Lee YB, Kim MA, *et al*. Effectiveness of nivolumab versus regorafenib in hepatocellular carcinoma patients who failed sorafenib treatment. *Clin Mol Hepatol* 2020;26:328–39.
5 Sung PS, Jang JW, Lee J, *et al*. Real-world outcomes of nivolumab in patients with unresectable hepatocellular carcinoma in an endemic area of hepatitis B virus infection. *Front Oncol* 2020;10:1043.
6 Greten TF, Abou-Alfa GK, Cheng A-L, *et al*. Society for immunotherapy of cancer (SITC) clinical practice guideline on immunotherapy for the treatment of hepatocellular carcinoma. *J Immunother Cancer* 2021;9:e002794.
7 Sung P-S, Kim C-M, Cha J-H, *et al*. A unique immune-related gene signature represents advanced liver fibrosis and reveals potential therapeutic targets. *Biomedicines* 2022;10:180. doi:10.3390/biomedicines10010180
8 Kazankov K, Jørgensen SMD, Thomsen KL, *et al*. The role of macrophages in nonalcoholic fatty liver disease and nonalcoholic steatohepatitis. *Nat Rev Gastroenterol Hepatol* 2019;16:145–59.
9 Sookoian S, Pirola CJ. Precision medicine in nonalcoholic fatty liver disease: new therapeutic insights from genetics and systems biology. *Clin Mol Hepatol* 2020;26:461–75.
10 Sung PS. Crosstalk between tumor-associated macrophages and neighboring cells in hepatocellular carcinoma. *Clin Mol Hepatol* 2021:308. doi:10.3350/cmh.2021.0308
11 MacParland SA, Liu JC, Ma X-Z, *et al*. Single cell RNA sequencing of human liver reveals distinct intrahepatic macrophage populations. *Nat Commun* 2018;9:4383.
12 Keenan BP, Fong L, Kelley RK. Immunotherapy in hepatocellular carcinoma: the complex interface between inflammation, fibrosis, and the immune response. *J Immunother Cancer* 2019;7:267.
13 Sun Y, Wu L, Zhong Y, *et al*. Single-cell landscape of the ecosystem in early-relapse hepatocellular carcinoma. *Cell* 2021;184:404–21.
14 Chen D-P, Ning W-R, Jiang Z-Z, *et al*. Glycolytic activation of peritumoral monocytes fosters immune privilege via the PFKFB3-PD-L1 axis in human hepatocellular carcinoma. *J Hepatol* 2019;71:333–43.
15 Chen D-P, Ning W-R, Li X-F, *et al*. Peritumoral monocytes induce cancer cell autophagy to facilitate the progression of human hepatocellular carcinoma. *Autophagy* 2018;14:1335–46.
16 Coelho I, Duarte N, Barros A, *et al*. Trem-2 promotes emergence of restorative macrophages and endothelial cells during recovery from hepatic tissue damage. *Front Immunol* 2020;11:616044.
17 Carpino G, Del Ben M, Pastori D, *et al*. Increased liver localization of lipopolysaccharides in human and experimental NAFLD. *Hepatology* 2020;72:470–85.
18 Cheng D, Chai J, Wang H, *et al*. Hepatic macrophages: key players in the development and progression of liver fibrosis. *Liver Int* 2021;41:2279–94.
19 Yao W, Ba Q, Li X, *et al*. A natural CCR2 antagonist relieves tumor-associated macrophage-mediated immunosuppression to produce a therapeutic effect for liver cancer. *EBioMedicine* 2017;22:58–67.
20 Ramachandran P, Dobie R, Wilson-Kanamori JR, *et al*. Resolving the fibrotic niche of human liver cirrhosis at single-cell level. *Nature* 2019;575:512–8.

21 Shalapour S, Lin X-J, Bastian IN, *et al*. Inflammation-induced IgA+ cells dismantle anti-liver cancer immunity. *Nature* 2017;551:340–5.

22 Hansen IS, Hoepel W, Zaat SAJ, *et al*. Serum IgA immune complexes promote proinflammatory cytokine production by human macrophages, monocytes, and Kupffer cells through FcαRI-TLR cross-talk. *J Immunol* 2017;199:4124–31.

23 Yi M, Niu M, Xu L, *et al*. Regulation of PD-L1 expression in the tumor microenvironment. *J Hematol Oncol* 2021;14:10.

24 Park D-J, Sung P-S, Lee G-W, *et al*. Preferential expression of programmed death ligand 1 protein in tumor-associated macrophages and its potential role in immunotherapy for hepatocellular carcinoma. *Int J Mol Sci* 2021;22:22094710. doi:10.3390/ijms22094710

25 Pfister D, Núñez NG, Pinyol R, *et al*. NASH limits anti-tumour surveillance in immunotherapy-treated HCC. *Nature* 2021;592:450–6.

26 Sung PS, Cheon H, Cho CH, *et al*. Roles of unphosphorylated ISGF3 in HCV infection and interferon responsiveness. *Proc Natl Acad Sci U S A* 2015;112:10443–8.

27 Sung PS, Cho SW, Lee J, *et al*. Infiltration of T cells and programmed cell death ligand 1-expressing macrophages as a potential predictor of lenvatinib response in hepatocellular carcinoma. *J Liver Cancer* 2020;20:128–34.

28 Cancer Genome Atlas Research Network. Electronic address WBE, cancer genome atlas research N. comprehensive and integrative genomic characterization of hepatocellular carcinoma. *Cell* 2017;169:1327–41.

29 Ma L, Hernandez MO, Zhao Y, *et al*. Tumor cell biodiversity drives microenvironmental reprogramming in liver cancer. *Cancer Cell* 2019;36:418–30.

30 Wang H, Feng C, Lu M, *et al*. Integrative single-cell transcriptome analysis reveals a subpopulation of fibroblasts associated with favorable prognosis of liver cancer patients. *Transl Oncol* 2021;14:100981.

31 Park DJ, Sung PS, Kim J-H, *et al*. EpCAM-high liver cancer stem cells resist natural killer cell-mediated cytotoxicity by upregulating CEACAM1. *J Immunother Cancer* 2020;8:e000301.

32 Heineke MH, van der Steen LPE, Korthouwer RM, *et al*. Peptide mimetics of immunoglobulin A (IgA) and FcαRI block IgA-induced human neutrophil activation and migration. *Eur J Immunol* 2017;47:1835–45.

33 Abeles RD, McPhail MJ, Sowter D, *et al*. CD14, CD16 and HLA-DR reliably identifies human monocytes and their subsets in the context of pathologically reduced HLA-DR expression by CD14(hi)/CD16(neg) monocytes: Expansion of CD14(hi)/CD16(pos) and contraction of CD14(lo)/CD16(pos) monocytes in acute liver failure. *Cytometry A* 2012;81:823–34.

34 Zhang Q, He Y, Luo N, *et al*. Landscape and dynamics of single immune cells in hepatocellular carcinoma. *Cell* 2019;179:829–45.

35 Zheng C, Zheng L, Yoo J-K, *et al*. Landscape of infiltrating T cells in liver cancer revealed by single-cell sequencing. *Cell* 2017;169:1342–56.

36 Mulder K, Patel AA, Kong WT, *et al*. Cross-tissue single-cell landscape of human monocytes and macrophages in health and disease. *Immunity* 2021;54:1883–900.

37 Wu C, Lin J, Weng Y, *et al*. Myeloid signature reveals immune contexture and predicts the prognosis of hepatocellular carcinoma. *J Clin Invest* 2020;130:4679–93.

38 McPherson S, Henderson E, Burt AD, *et al*. Serum immunoglobulin levels predict fibrosis in patients with non-alcoholic fatty liver disease. *J Hepatol* 2014;60:1055–62.

39 Liu WT, Jing YY, Han ZP, *et al*. The injured liver induces hyperimmunoglobulinemia by failing to dispose of antigens and endotoxins in the portal system. *PLoS One* 2015;10:e0122739.

40 Shalapour S, Font-Burgada J, Di Caro G, *et al*. Immunosuppressive plasma cells impede T-cell-dependent immunogenic chemotherapy. *Nature* 2015;521:94–8.

41 Grierson P, Crites D, Ruzinova MB, *et al*. Distinct clinical and magnetic resonance features of metastatic hepatocellular carcinoma treated with pembrolizumab: a case report of late response after pseudoprogression. *Hepatol Commun* 2018;2:148–51.

42 Liu Y, Wang X, Yang Y. Hepatic Hippo signaling inhibits development of hepatocellular carcinoma. *Clin Mol Hepatol* 2020;26:742–50.

43 Janse van Rensburg HJ, Azad T, Ling M, *et al*. The Hippo pathway component TAZ promotes immune evasion in human cancer through PD-L1. *Cancer Res* 2018;78:1457–70.

44 Yang W, Yang S, Zhang F, *et al*. Influence of the Hippo-YAP signalling pathway on tumor associated macrophages (TAMs) and its implications on cancer immunosuppressive microenvironment. *Ann Transl Med* 2020;8:399.

45 Zhou X, Li W, Wang S, *et al*. YAP aggravates inflammatory bowel disease by regulating M1/M2 macrophage polarization and gut microbial homeostasis. *Cell Rep* 2019;27:1176–89.

46 Kim W, Khan SK, Liu Y, *et al*. Hepatic Hippo signaling inhibits protumoural microenvironment to suppress hepatocellular carcinoma. *Gut* 2018;67:1692–703.

47 Zhang X, Li Y, Ma Y, *et al*. Yes-associated protein (YAP) binds to HIF-1α and sustains HIF-1α protein stability to promote hepatocellular carcinoma cell glycolysis under hypoxic stress. *J Exp Clin Cancer Res* 2018;37:216.

48 Moya IM, Castaldo SA, Van den Mooter L, *et al*. Peritumoral activation of the Hippo pathway effectors YAP and TAZ suppresses liver cancer in mice. *Science* 2019;366:1029–34.